Planet. Space Sci., Vol. 37, No. 11, pp. 1347–1365, 1989
Printed in Great Britain.

0032-0633/89 $3.00 + 0.00
Pergamon Press plc

INTERPLANETARY MAGNETIC FIELD CONTROL OF DAYSIDE AURORAL ACTIVITY AND THE TRANSFER OF MOMENTUM ACROSS THE DAYSIDE MAGNETOPAUSE

M. LOCKWOOD*
Rutherford Appleton Laboratory, Chilton, Didcot, Oxon OX11 0QX, U.K.

P. E. SANDHOLT
Department of Physics, University of Oslo, Box 1048, Blindern, 0316 Oslo 3, Norway

S. W. H. COWLEY
Blackett Laboratory, Imperial College, London SW7 2BZ, U.K.

and

T. OGUTI
Geophysics Research Laboratory, University of Tokyo, Bunkyo-ku, Tokyo, 113, Japan

(*Received* 25 *April* 1989)

Abstract—The orientation of the Interplanetary Magnetic Field (IMF) during transient bursts of ionospheric flow and auroral activity in the dayside auroral ionosphere is studied, using data from the EISCAT radar, meridian-scanning photometers, and an all-sky TV camera, in conjunction with simultaneous observations of the interplanetary medium by the *IMP*-8 satellite. It is found that the ionospheric flow and auroral burst events occur regularly (mean repetition period equal to 8.3 ± 0.6 min) during an initial period of about 45 min when the IMF is continuously and strongly southward in GSM coordinates, consistent with previous observations of the occurrence of transient dayside auroral activity. However, in the subsequent 1.5 h, the IMF was predominantly northward, and only made brief excursions to a southward orientation. During this period, the mean interval between events increased to 19.2 ± 1.7 min. If it is assumed that changes in the North–South component of the IMF are aligned with the IMF vector in the ecliptic plane, the delays can be estimated between such a change impinging upon *IMP*-8 and the response in the cleft ionosphere within the radar field-of-view. It is found that, to within the accuracy of this computed lag, each transient ionospheric event during the period of predominantly northward IMF can be associated with a brief, isolated southward excursion of the IMF, as observed by *IMP*-8. From this limited period of data, we therefore suggest that transient momentum exchange between the magnetosheath and the ionosphere occurs quasi-periodically when the IMF is continuously southward, with a mean period which is strikingly similar to that for Flux Transfer Events (FTEs) at the magnetopause. During periods of otherwise northward IMF, individual momentum transfer events can be triggered by brief swings to southward IMF. Hence under the latter conditions the periodicity of the events can reflect a periodicity in the IMF, but that period will always be larger than the minimum value which occurs when the IMF is strongly and continuously southward.

1. INTRODUCTION

The discovery of characteristic magnetic field signatures near the dayside magnetopause, principally recognized by a bi-polar variation in the boundary-normal component, was made by Russell and Elphic (1978, 1979) using data from the *ISEE*-1 and -2 satellites. These authors interpreted the observations in terms of transient events of magnetic flux transfer during which previously closed geomagnetic field-lines were connected to the Interplanetary Magnetic Field (IMF) and hence termed them "Flux Transfer Events" (FTEs). Independently, Haerendel *et al.* (1978) recognized these events in plasma and magnetic field data from the *Heos*-2 spacecraft and called them "flux erosion events". More recent work has shown that there is much structure associated with FTEs in terms of ion populations, streaming hot electrons, wave emissions and field boundary layers (e.g. Farrugia *et al.*, 1988), providing tight constraints for any model of FTE formation and evolution. Russell and Elphic introduced a model of FTEs which assumed that reconnection at the dayside magneto-

*Also Visiting Honorary Lecturer, Imperial College, London SW7 2BZ, U.K.

pause could be patchy in space and variable in time, such that an isolated reconnected flux tube, of roughly circular cross-section, was produced and then dragged over the magnetopause. More recently, several authors have questioned if the reconnection is necessarily so spatially localized and suggested that the newly-reconnected field-lines may thread a region which is elongated in the direction perpendicular to its motion across the magnetopause. Lee and Fu (1985) and Lee *et al.* (1988) suggested the existence of elongated multiple neutral lines at which reconnection occurs (necessarily in a time-varying manner). However, it appears that such a situation could give rise, with equal frequency, to twisted flux tubes which are connected at either end to the IMF, to the Earth at both ends, or are connected to the IMF at one end and to the Earth at the other. Southwood *et al.* (1988) and Scholer (1988) have shown that the magnetic perturbations at the magnetopause could arise from variations in reconnection rate at a single long neutral line. These theories have the advantage of explaining the occurrence of continued streams of hot electrons on field-lines at the edge of the FTE because these map back to a neutral line where reconnection can continue after the formation of the FTE. In the Southwood *et al.* (1988) and Scholer (1988) models, the original concept of Russell and Elphic is maintained in that magnetospheric flux tubes are connected at one end to the IMF, giving the mixture of magnetosheath and magnetospheric plasma which is observed in the central region of FTEs.

The major difference between the predictions of these models of FTEs is the total magnetic flux transferred from closed to open in each event, the Russell and Elphic model giving lower values than the others. (Note, however, that this is offset by the possibility that several events could occur simultaneously in the Russell and Elphic model.) An FTE model is required because as a newly opened flux tube moves over a satellite near the magnetopause, its dimension in the direction perpendicular to that motion cannot be determined. The choice of model therefore alters any estimate of the total voltage applied across the magnetosphere, and hence across the ionospheric polar cap, by these events. As a result, their significance as a driving mechanism for ionospheric high-latitude convection is not yet wholly clear. Some information on the unknown dimension has been gained from the *ISEE*-1 and -2 satellites when well separated at the magnetopause (e.g. Saunders *et al.*, 1984); however, ground-based observations offer the best opportunity to quantify the potential by defining the extent and velocity of the ionospheric foot of the newly-opened flux tube. Predictions of the ionospheric flow and current signatures which would be expected for some of these models of magnetopause FTEs have been made by Southwood (1985, 1987) and Cowley (1986).

The detection of FTE signatures in data from ground-based magnetometers (as modelled by McHenry and Clauer, 1987) has proven very difficult, although some possible events have been identified (Lanzerotti *et al.*, 1987). However, Farrugia *et al.* (1989) have shown that the same signature at any one station can be produced by dynamic pressure changes in the solar wind. These authors also directly observed the related magnetopause motions caused by the solar wind changes. Hence such signatures need not be associated with reconnection at all. In addition, Sibeck *et al.* (1989) have recently shown that other magnetometer deflections which could be interpreted as FTE signatures are, at least sometimes, associated with dynamic pressure changes in the solar wind. Lockwood *et al.* (1989a) have pointed out that the simplifying assumptions in the model predictions may well be responsible for the lack of clear FTE signatures in ground-based magnetometer data, bearing in mind that a magnetometer integrates the current pattern over an extended region of radius up to about 300 km. Chief among these reasons are: the fact that events do not move over a station with a constant velocity; that the precipitation associated with each event means that conductivity is far from uniform and highly time dependent; that events tend to occur in series and the effects of one event are superposed on those of the previous event; and that event lifetimes are shorter than, or comparable with, the time taken for an event to traverse the region to which a magnetometer station is sensitive.

Data from ground-based radars, however, provide a direct measure of electric field within a small scattering volume. Observations from VHF coherent radars are subject to some uncertainties when the electric field is large. Nevertheless, Goertz *et al.* (1985) found examples of STARE radar data showing transient flows into the polar cap, associated with particle dropouts observed by the conjugate *GEOS* satellite. These authors showed both sets of signatures were consistent with FTE behaviour. Todd *et al.* (1986, 1988) also observed large impulsive poleward flow bursts in the dayside auroral zone and were able to show that the dipolar line-of-sight velocity variations within each range gate were all in very good agreement with the twin-vortical Southwood (1985, 1987) model of an ionospheric signature of an FTE. Kokubun *et al.* (1988) have shown that the events observed using the EISCAT radar are accompanied by impulsive spikes in local magnetometer records, similar to those

reported by Lanzerotti *et al.* (1987), but not in complete agreement with the simplified model predictions of McHenry and Clauer (1987). However, as with the magnetometer data, Sibeck *et al.* (1989) have shown that these radar signatures may well have been caused by a pulse of solar wind dynamic pressure. The Goertz *et al.* and Farrugia *et al.* papers relate ionospheric electric field variations to changes at the magnetopause.

However, as yet no simultaneous observations of an FTE (meaning here a direct measurement of a bipolar oscillation in the boundary normal field and all attendant particle and field signatures) and a coincident ionospheric flow burst have been made, despite several attempts to find such a case (R. C. Elphic, private communication, 1988). This may be because the probability of both the radar field-of-view and the satellite being sufficiently close to an FTE at the same time is very low. In addition, the ionospheric signature of an FTE may not appear until after the magnetopause signature has disappeared if IMF B_y is small (Lockwood and Freeman, 1989; Lockwood and Cowley, 1988). In conclusion, although the FTE models of Russell and Elphic (1979), Lee and Fu (1985), Southwood *et al.* (1988) and Scholer (1988) all require that an FTE generate flow and current signatures in the ionosphere, there has been no clear and consistent evidence for such effects. The ability of dynamic pressure changes to mimic the predictions of certain models has added to the confusion concerning the identification of FTE effects in the ionosphere.

Another ionospheric phenomenon which it has been suggested is related to FTEs is the formation of transient dayside auroral arcs and arc fragments, which has been termed "dayside auroral breakup" (Sandholt *et al.*, 1985, 1989a; Sandholt, 1988). These events are observed at all local times in the dayside auroral oval by both meridian-scanning photometers and all-sky TV cameras (Sandholt *et al.*, 1989b) and are also associated with impulsive spikes in local magnetometer records (Oguti *et al.*, 1988). Recently, Lockwood *et al.* (1989a) showed that these optical events were indeed associated with impulsive flow bursts in the ionosphere, as observed by the EISCAT radar. Furthermore, Sandholt *et al.* (1989b) have shown that the arcs at all times move with a velocity approximately equal to the ion drift simultaneously observed by the radar. This gives two ways in which event potential can be deduced from these measurements. The first is using the observed velocity and extent of the optical arc, which can be done because the arc is now known to be moving with a velocity $\mathbf{E} \times \mathbf{B}/B^2$. Alternatively, the electric field observed by the radar can be integrated over the field-of-view. The results give potentials associated with these ionospheric events of 30–60 kV—rather larger than the Russell and Elphic model would predict from the magnetopause measurements, but more consistent with predictions for the elongated neutral line models of Lee and Fu (1985), Scholer (1988) and Southwood *et al.* (1988). In addition, the above observed potentials are minima as they refer to the potential along the visible arc or applied across the EISCAT radar field-of-view, neither of which may define the full extent of the event. Using supporting information from a chain of magnetometers, the full potential associated with the largest of the events is estimated to be at least 80 kV (Lockwood *et al.*, 1989a).

The strongest evidence for the association of the dayside auroral events and magnetopause FTEs comes from their occurrence and repetition period (see review by Sandholt, 1988) and the fact that events (in the Northern Hemisphere) move westward during positive IMF B_y and eastward when it is negative, as expected for a reconnection phenomenon (Jørgensen *et al.*, 1972; Cowley, 1981). Furthermore, the events move West/East initially before moving poleward and this behaviour is also noted in the simultaneous radar data (Lockwood *et al.*, 1989a; Sandholt *et al.*, 1989b). This is as predicted for a newly-opened flux tube by Lockwood and Freeman (1989) and Saunders (1989) because magnetic tension effects associated with IMF B_y can commence in the ionosphere before the anti-solar pull of the solar wind becomes effective.

Some of the known features of the occurrence of the dayside auroral breakup phenomenon are displayed in Fig. 1, which surveys all the limited observations published to date. Part (a) shows the number of full 30 min periods of clear-sky, 630 nm photometer observations from Ny Ålesund, Spitsbergen for which the persistant, background dayside aurora falls in the given 1° bins of geomagnetic latitude. Only data from days during which transient auroral arcs are observed are included. These data have been accrued over a number of winter observing seasons and examples of the transient events are presented in a variety of publications (Sandholt *et al.*, 1985; 1989a,b,c; Sandholt, 1988; Sandholt and Egeland, 1988; Lockwood *et al.*, 1989a). Part (b) of Fig. 1 presents the average number of dayside auroral breakup events per 30 min period as a function of the geomagnetic latitude of the background aurora. It can be seen that the transient events are most common when the background aurora is close to its southernmost position, but are absent when it is at its most northerly position. Note that the exclusion of days without any transient arcs excludes many observations at higher latitudes in part (a) of Fig. 1. A comprehensive survey of all available data

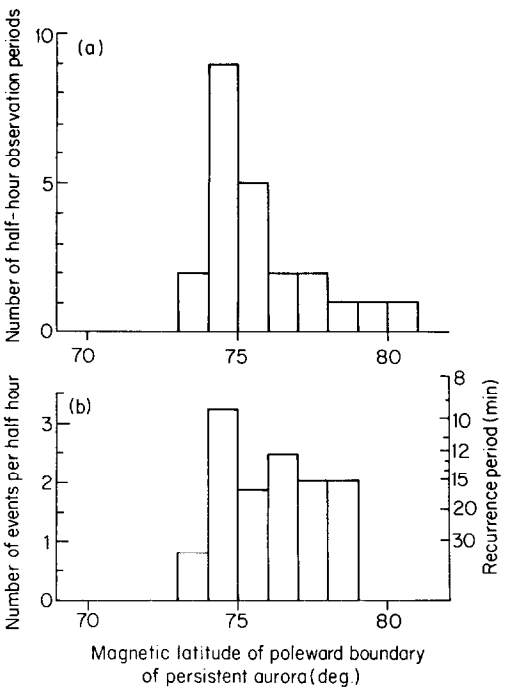

FIG. 1. STATISTICS OF OBSERVATIONS OF "DAYSIDE AURORAL BREAKUP" EVENTS.

(a) Numbers of full, cloud-free, 30 min observation periods of the dayside aurora from Ny Ålesund, Spitsbergen, for which the persistent dayside aurora fell within the given 1° bins of geomagnetic latitude. (b) The mean number of "dayside auroral breakup" transient events per 30 min period for the same bins of the geomagnetic latitude of the persistent background aurora.

will be presented at a later date. The peak occurrence rate is 3.2 events per 30 min period, i.e. a recurrence period of 9.4 min. These limited data do indirectly suggest a dependence of transient events on IMF B_z, with events being more common for the southerly auroral positions expected for southward IMF. However, there is an indication of a cut-off in event occurrence when the background aurora moves poleward of 79° (roughly corresponding to northward IMF).

Like more steady forms of reconnection at the low-latitude magnetopause, FTEs are known to occur almost always during southward IMF, i.e. when B_z is negative (see reviews by Cowley, 1982, 1984). This was established by Rijnbeek *et al.* (1984) who employed data on FTEs from the *ISEE* satellites, both in the magnetosheath and just inside the magnetosphere and sorted events according to the sheath field. A similar result was obtained by Berchem and Russell (1984), who only employed FTE data from the *ISEE* satellites when in the magnetosheath and compared with the orientation of the undisturbed IMF. These studies indicate that negative IMF B_z is very nearly a necessary and sufficient condition for the occurrence of FTEs at the magnetopause. Rijnbeek *et al.* showed that when $B_z < 0$, FTEs occur with a mean recurrence period of 7 min but are absent when $B_z > 0$. Similar results were obtained with a slightly longer recurrence period by Berchem and Russell, the small differences probably being associated with a more restrictive definition of an FTE signature. Data from the *AMPTE–UKS* satellite give somewhat lower occurrence frequencies, thought to be because this satellite surveyed the magnetopause at lower latitudes (Southwood *et al.*, 1986). The occurrence of transients in the dayside aurora therefore has strong similarities to that of magnetopause FTEs.

In this paper we employ the only available combined radar and optical data, i.e. from the period recently reported by Lockwood *et al.* (1989a), to investigate the occurrence of the transient auroral/flow burst events (as studied in detail by Sandholt *et al.*, 1989b) and their relationship to the B_z-component of the interplanetary magnetic field. Results are then compared with the surveys of FTE occurrence discussed above.

2. OBSERVATIONS

2.1. *Ground-based radar, optical and magnetometer data*

Parts (a)–(d) of Fig. 2 show sequences of data from meridian-scanning photometers at Ny Ålesund (NA), Spitsbergen, along with vector ion flow data observed by the EISCAT radar, as a function of Universal Time. Part (e) is an image from an all-sky TV camera, also at Ny Ålesund, projected onto a geographic latitude–longitude frame, using an assumed emission altitude of 130 km. These data were recorded between 09:05 and 09:30 U.T. on 12 January 1988 (M.L.T. ≈ 12:00–12:30), and the image (e) is taken during a 2-s integration period ending at 09:20:55 U.T. Together, these data illustrate the typical features of the transient burst events of auroral activity and ion flow.

If we firstly consider the image [part (e) of the figure], the locations of three magnetometers are marked: Ny Ålesund (NA), Hornsund (H) and Bjørnøya (B). Also shown (dot-and-dash line) is the meridian scanned every 18 s by photometers at Ny Ålesund. The results of these scans are given in panels (a) and (b) for wavelengths of 630 and 557.7 nm, respectively (i.e. red and green line auroral emissions). The received intensity is shown as a function of zenith angle at Ny Ålesund, and at the top of each panel the approximate locations of the three magnetometer

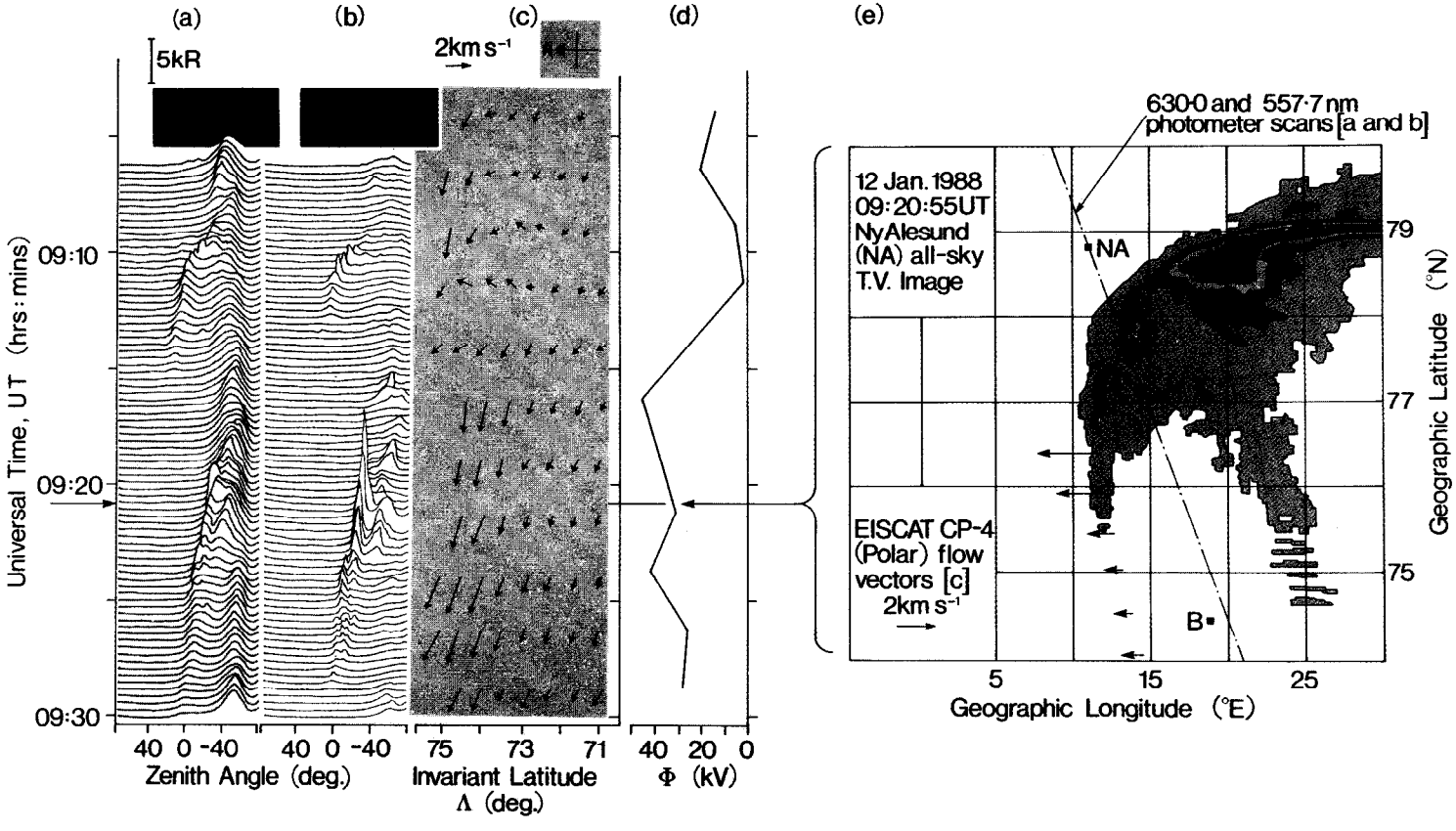

FIG. 2. (a–e) EXAMPLES OF TRANSIENT DAYSIDE AURORAL/FLOW-BURST EVENTS, OBSERVED BY THE EISCAT RADAR, PHOTOMETERS AND ALL-SKY TV CAMERA ON 12 JANUARY 1988.

Auroral luminosity is shown as a function of U.T. and zenith angle (positive to the North) by the (a) 630 nm and (b) 557.7 nm meridian-scanning photometers at Ny Ålesund (NA). Panel (c) gives the ion drift velocities observed by EISCAT, and (d) the potential across the North–South dimension of the EISCAT field-of-view (Φ). The all-sky TV image at 09:20:55 is given in (e), which also shows the near-simultaneous EISCAT flow data, the meridian scanned by the photometers (dot–dash line) and the locations of magnetometers at Hornsund (H) and Bjørnøya (B), the approximate zenith angles of which are also indicated at the top of (a) and (b).

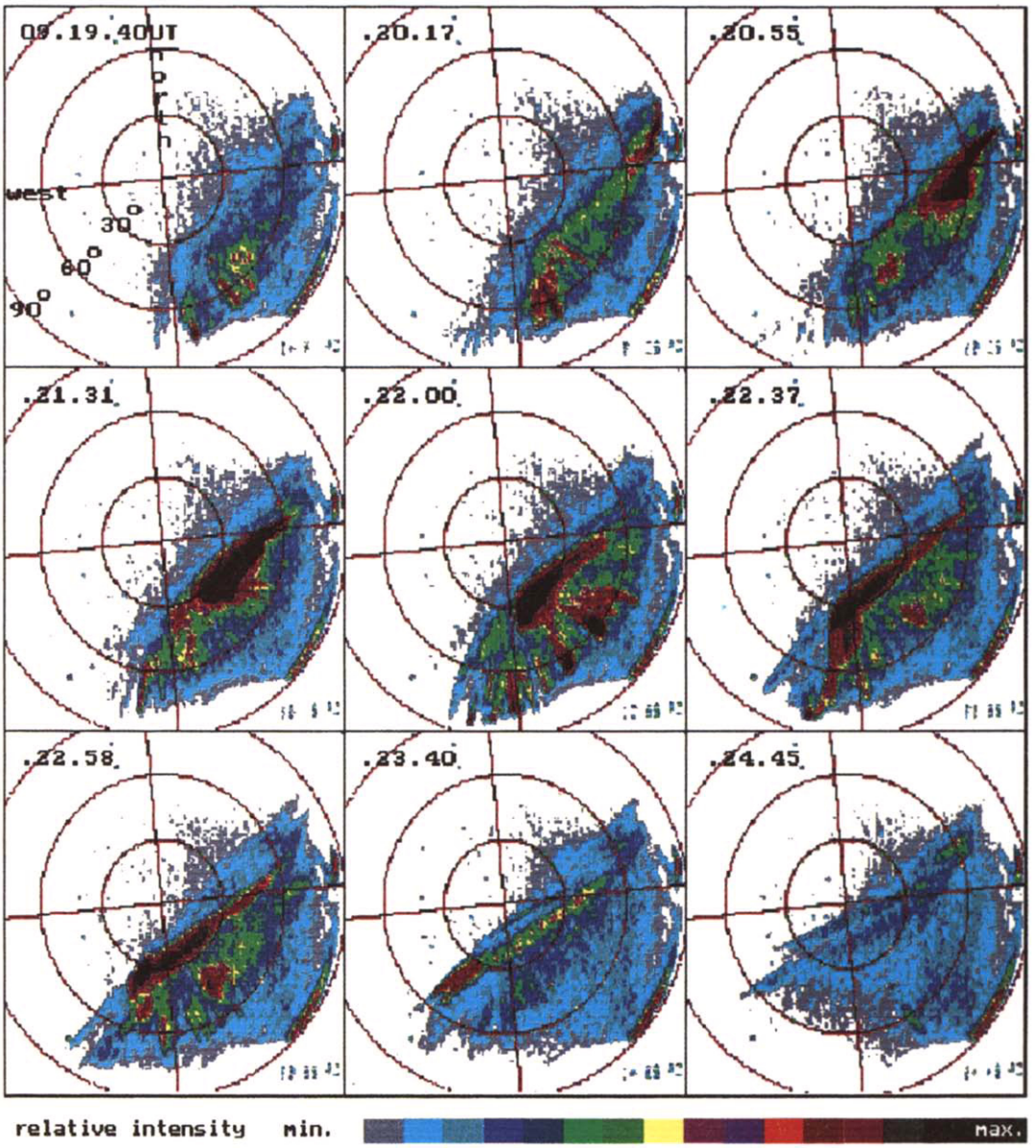

FIG. 2. (f) THE SEQUENCE OF FALSE-COLOUR ALL-SKY TV CAMERA IMAGES (2 S INTEGRATIONS) BETWEEN 09:19:40 U.T. AND 09:24:45 U.T. (THE THIRD IMAGE, FOR 09:20:55 U.T., IS ALSO REPRODUCED IN FIG. 2(e) ON A REGULAR GRID).
The circles are constant zenith angles, and the axes geographic North and West, at Ny Ålesund.

stations (NA, H and B) are given: these are calculated assuming emission altitudes of 130 and 250 km for the green and red line, respectively. Further details of the photometer observations are given by Sandholt *et al.* (1985, 1989a,b,c).

Also shown in part (e) of Fig. 2 is the set of flow vectors observed by the EISCAT radar at the time closest to that when the all-sky image was recorded (i.e. for 09:21:15). The radar was operating in Common Programme CP-4, which is virtually identical to the U.K.-POLAR programme described by van Eyken *et al.* (1984) and Willis *et al.* (1986). This mode employs beamswinging between two azimuths 24° apart, at low elevations to the north of the radar. The beamswinging cycle time is 5 min and vectors are obtained every 2.5 min by linearly interpolating the line-of-sight data from one azimuth between successive antenna dwells and then comparing with the observed value for the interim dwell at the other azimuth. The vectors are ascribed to the points midway between the two azimuths, the locations of which can be seen in part (e) of Fig. 2. Panel (c) shows the vectors as a function of time and invariant latitude. Flows are seen to be large and westward in the northern half of the field-of-view, particularly during two periods when discrete auroral structures are observed by the photometers (09:08–09:13 and 09:18–09:27 U.T.). The westward flow corresponds to a northward electric field and, in order to quantify the total westward flow within the radar field of view, this electric field component has been integrated over the first seven gates observed by the radar to give the potential (Φ) which is plotted in panel (d) as a function of time.

If we consider the second (and larger) of the two events, we see that Φ rises sharply between 09:12 and 09:17 U.T., peaking just before the onset of the optical event, as seen in the red line scans (09:18 U.T.) and considerably before the onset of the event as seen in the green line scans (09:21:30 U.T.). The image (e) is taken between these two times. The TV camera is mainly sensitive to 557.7 nm (green line) emissions, and the peak luminosity is known from the sequence of 2-s images, given in Fig. 2f, to be moving westward at 3 km s^{-1} at 09:20 U.T. (very similar to the ion flow velocity observed by the radar at the same time). It can be seen that the peak green line emissions are slightly to the north of the radar field-of-view and that the band of enhanced ion flow is within the region of persistent cleft/cusp luminosity (from the photometers this is known to be mainly red line emission). Note that the exact locations of red line emissions in part (e) will be incorrect because of the assumption of an emission altitude of 130 km, and that the spur of low-level luminosity seen to the southeast of

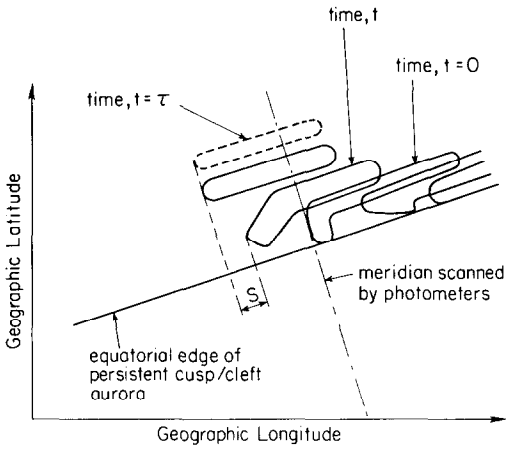

FIG. 3. SCHEMATIC OF THE MOTION OF THE PATCHES OF HIGH 557.7 nm LUMINOSITY OVER THE PHOTOMETER SCAN. Time $t = 0$ is when the event first crosses the meridian scanned and $t = \tau$ is the time when the event begins to move purely northward, with negligible westward (magnetic) flow, and fade (see Fig. 2f).

Hornsund (H) is due to scattered sunlight. Figure 3 shows schematically the evolution of the auroral structure observed by the all-sky TV cameras during the period 09:19–09:25 U.T. The locations of peak luminosity are shown at various U.T. relative to time $t = 0$ when the event reaches the photometer meridian (dot-and-dash line). Note that Fig. 2e corresponds to negative t and the second of the sequence of locations shown in Fig. 3. The event initially moves rapidly westward, the shape and motion of the event then evolves until it is elongated in the East–West direction and moving poleward. Finally the event fades as it moves into the polar cap and is no longer detectable in the photometer data by $t = \tau$ ($\approx$5–15 min). All events observed on 12 January 1988 showed the basic behaviour described in Fig. 3. From the onset times of the event, as seen in the TV camera, photometer and radar data, and the speed of the westward motion, we estimate that the event originated somewhere less than 650 km to the east of the longitude of the observations, i.e. between the centre of the afternoon M.L.T. sector and noon.

Further details of the events shown in Fig. 2, including a study of the magnetometer data from all local stations, are given by Sandholt *et al.* (1989b). The association of the peaks in Φ with the optical events has been demonstrated by Lockwood *et al.* (1989a) and is shown here in Fig. 4. The top panel shows the radar potential Φ discussed above, for the entire period when combined radar–optical observations were possible (09:00–11:20 U.T.). Part (b) of Fig. 4 shows the zenith angle of peak 630 nm emission, as

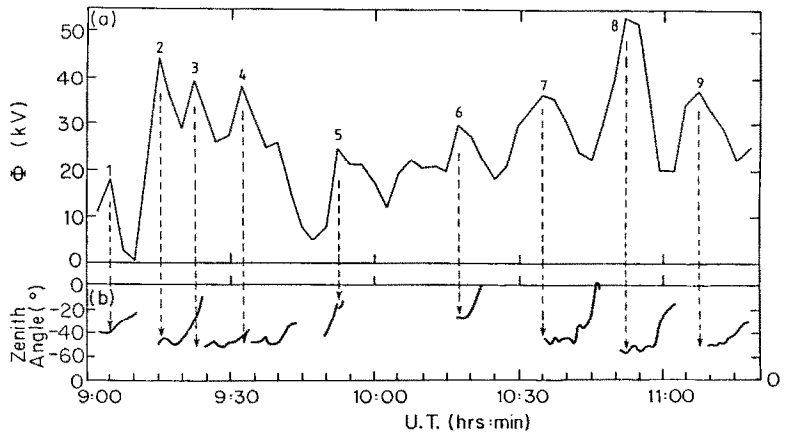

FIG. 4. TRANSIENT EVENTS ON 12 JANUARY 1988.
(a) Potential across the North–South dimension of the EISCAT field of view, Φ, and (b) zenith angle (at Ny Ålesund) of peak 630 nm emissions greater than 3 kR as a function of U.T. Events 1 and 2 are shown in more detail in Fig. 2.

observed by the photometer at Spitsbergen. In order to separate the transient events from the background cusp/cleft emissions, only peak intensities greater than 3 kR are shown. The dashed arrows indicate that each peak in the radar potential is close to the onset of a 630 nm event, considering the 2.5-min resolution of the radar data. In total, there were nine clear optical/flow burst events in this period, and these are numbered in Fig. 4. It should be noted that the flow bursts are substantially different in form from those reported by Todd *et al.* (1986, 1988) in that they are initially westward, have greater velocities (3–4 km s^{-1}) and longer durations (up to 10 min).

Figure 5 provides further evidence that the optical auroral and radar flow-burst events are associated. The peak radar potential during the initial westward-moving phase of each event is plotted as a function of the lifetime, τ, of the subsequent auroral event, as observed by the 630 nm meridian-scanning photometer. It can be seen that the longer-lived auroral events are indeed associated with larger potentials. The implications of this correlation will be discussed in Section 4.3.

It should be noted that the vector radar data are subject to errors introduced by the use of the beam-swinging technique. Care must be taken in their interpretation because changes are taking place over time scales comparable with the radar beam-swinging period. Etemadi *et al.* (1989) have modelled the effects of using this technique with step-function changes in real flow speed and have noted two effects. "Smoothing" causes the derived flow change to be spread over a period of time equal to the beam-swinging period (5 min for CP-4), while "mixing" causes a spurious component in the westward flow to be generated by real changes in the northward flow (and vice-versa). The nature of the spurious mixing effect depends on the phase of the real flow change with respect to the beam-swinging cycle, and hence we would expect a great variety in the behaviour of the derived vectors for each event, were mixing effects important. In Fig. 4, the peaks in Φ all occur close to the time of onset of a 630 nm arc, as seen by the photometers, the only exception to this being event 5, for which it occurs 2.5 min later (i.e. one Φ data point). In this paper, we are more concerned with the timing of the event onsets, rather than the velocities and

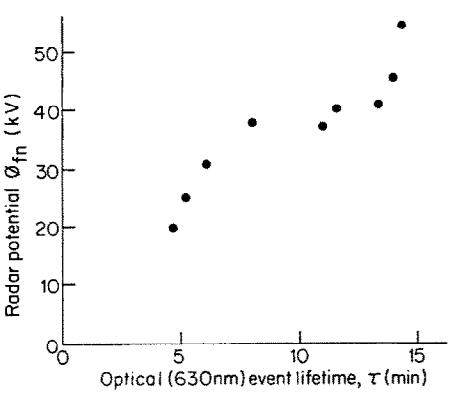

FIG. 5. POTENTIAL OBSERVED BY EISCAT, Φ, AS A FUNCTION OF THE EVENT LIFETIME, τ, OBSERVED BY THE 630 nm PHOTOMETER. The potential is across the North–South dimension of the field-of-view (corresponding to westward flow) and the optical lifetime is defined for emissions of intensity greater than 3 kR.

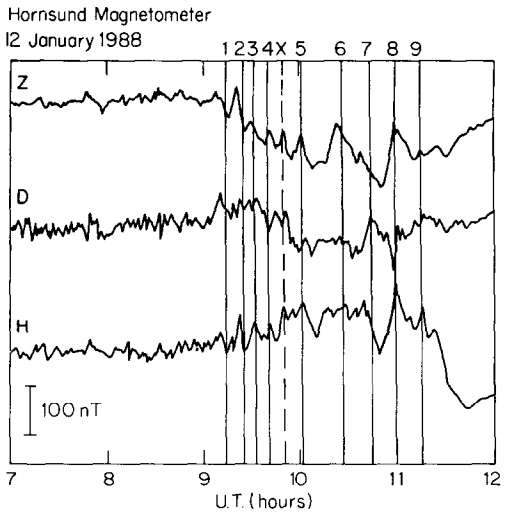

FIG. 6. MAGNETOGRAMS FROM HORNSUND (H IN FIG. 2) FOR 12 JANUARY 1988.
The times 1–9 refer to the event onsets shown in Fig. 4, lagged by 7 min.

potential magnitude in each event. The work of Etemadi *et al.* indicated that a response to a sudden change, as observed in derived vectors, could be shifted in time by up to half a beam-swing cycle (2.5 min), if mixing effects were large (but on averaging sufficient events this shift goes to zero). We do not expect significant mixing effects here as the optical and magnetometer data show that the initial onset of flow is westward, for which only smoothing effects are produced (see Etemadi *et al.*). Thus we take the peak Φ to be a good indicator of the time of the maximum flow in every event. The lack of variety of this time with respect to the onset of the 630 nm optical events strongly supports this assumption (see Fig. 4).

The sequence of events shown in Fig. 4 is also found in magnetometer data from Hornsund (H in Fig. 2, and the closest magnetometer to the auroral activity). These data are shown in Fig. 6. The numbered vertical lines correspond to the event numbers given in Fig. 4, but the times have been lagged by 7 min in Fig. 6 because, as discussed above, the radar potential peaks at a time close to the onset of the 630 nm event whereas the 557.7 nm luminosity does not increase until some 7 min later. The peak effect in the magnetometer record from Hornsund is almost coincident with the arrival of the 557.7 nm luminosity at the photometer meridian, implying that the conductivity changes associated with the arc are an important factor in establishing the magnetometer signature. It can be seen that close to each vertical line in Fig. 6, there is a well-defined peak in the Z-component in nearly all cases (the association is least clear for events 1, 7 and 9). Simultaneous deflections are often observed in the other components (D and H), however the sequence is more complex than that seen in Z. Because the difference in the times of peak electric field and auroral luminosity (and conductivity) is not the same for each event, we should expect this variety of magnetic field signatures. However, Fig. 6 is consistent with a quasi-periodic intensification of eastward current to the north of the station. In fact, these magnetometer data reveal an additional event, X. This event is not distinguished in Fig. 4 because the intensity of 630 nm emissions between events 4 and X does not fall below 3 kR. Careful inspection of Fig. 4 does reveal a small peak in Φ near 09:40 U.T. (7 min before the additional pulse X in the magnetometer data from Hornsund) following an equatorward step in the peak 630 nm emissions. We conclude that event X was in all likelihood an event of the same kind as 1–9. In Section 3 we shall consider the event repetition period, both excluding and including event X.

Sandholt *et al.* (1989b) have presented the magnetometer data from the other local stations (Ny Ålesund, Bjørnøya and Tromsø) and have shown that the deflections are consistent with a series of travelling twin-vortical flow patterns, as described by Lockwood *et al.* (1989a). Figure 7 shows the evolution of these events schematically for the Northern Hemisphere. The events discussed in this paper were all observed while the duskwards (B_y)-component of the IMF was large and positive and all initially move rapidly westward from about 14:00 M.L.T. to near noon. Note that the events have a sunward component of velocity in this initial phase of motion, which Lockwood *et al.* (1989a) associate with the effect of magnetic tension on newly-reconnected flux tubes. This tension effect acts before any anti-solar motion is produced in the ionosphere by the magnetosheath flow (Lockwood and Freeman, 1989; Saunders, 1989). The newly-opened flux tube is shown as circular in Fig. 7 for simplicity and as it moves it creates a twin-vortical flow pattern, as predicted by Southwood (1985, 1987), Southwood *et al.* (1988) and Cowley (1986). The 557.7 nm arcs and arc-fragments are found within the inferred region of upward field-aligned currents. This current is one of the oppositely-directed pair on the flanks of the newly-reconnected flux tube which transfer momentum down into the ionosphere. Hence precipitating electrons could both produce the arc and be the current carriers for the momentum transfer. The $B_y > 0$ events are observed to move westward through noon before "peeling off" the polar cap boundary and moving into the polar cap, as predicted by Saunders (1989).

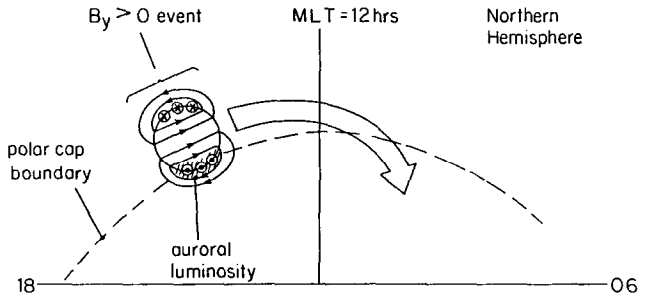

FIG. 7. SCHEMATIC OF MOTION OF NEWLY RECONNECTED FLUX TUBES, CAUSING TWIN VORTICAL FLOW PATTERNS, CONSISTENT WITH THE RADAR, TV CAMERA, PHOTOMETER AND MAGNETOMETER DATA. Events are shown in the Northern Hemisphere for positive IMF B_y.

2.2. *IMF and solar wind data*

During the period discussed in this paper, the Interplanetary Magnetic Field (IMF) was monitored by the *IMP*-8 satellite, along with the solar wind density and flow velocity. The *IMP*-8 satellite was in a position outside the dawn flank of the magnetosphere, in the solar wind, as shown schematically in Fig. 8. The exact locations of the spacecraft in GSE coordinates are given in Table 1, for the times of the events as numbered in Fig. 4. In all cases the satellite Z-coordinate was close to $6R_E$. In order to estimate the propagation delays for changes in the IMF observed by *IMP*-8 to reach the subsolar magnetopause, we require some knowledge of the solar wind flow. The available solar wind data for this day are plotted in Fig. 9. The period marked O is when the combined radar/optical observations were made. It can be seen that only two reliable solar wind data points are available in this period, both near 09:00 U.T. The solar wind and IMF data both show that a weak bow shock passed over the spacecraft near 04:15 U.T. placing *IMP*-8 in the magnetosheath until 05:15 U.T., when the bow shock moved back across the spacecraft. From shortly after this time, the solar wind data are missing; however, the IMF data show the spacecraft to remain in the unshocked solar wind for the remainder of the day, although the presence of upstream waves shows that the satellite remained close to the bow shock during the period O. The data show that an increase in the solar wind speed and a decrease in the density took place during the data gap. For the purpose of predicting the magnetopause location, we have linearly interpolated the data across the data gap and the period when *IMP*-8 was in the sheath, as shown by the dashed lines in Fig. 9: the few available data points are close to the interpolated values obtained in this way.

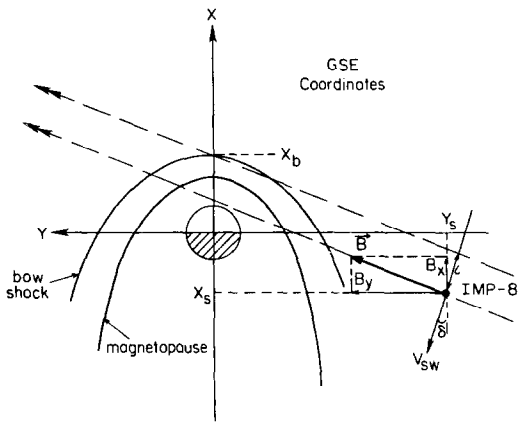

FIG. 8. RELATIVE LOCATIONS OF *IMP*-8 SATELLITE, BOW SHOCK AND MAGNETOPAUSE.
The figure is not to scale but shows the geometry used in calculation of delays. Note that, although shown here in ortho-garden hose orientation in order that the terms in equation (5) be derived with the correct senses, the IMF during the events studied had $B_y > 0$ and $B_x < 0$ (see Table 1).

For this satellite position on the flanks of, and just upstream from, the Earth's bow shock, it is difficult to evaluate accurately the delay between a change in the IMF impinging upon the satellite and its effects reaching the ionosphere within the radar field-of-view.

Such a delay will have four components: a lag T_{sb} between the change reaching the satellite and the subsolar bow shock; a time T_{bm} during which the change propagates across the magnetosheath to the subsolar magnetopause; a lag T_{mi} for the effect of any variation in reconnection rate to reach the cleft ionosphere; and finally a delay T_{ir}, during which the effect propagates into the radar field-of-view. The total delay is thus (Lockwood and Cowley, 1988; Farrugia *et al.*, 1989):

$$T_{sr} = T_{sb} + T_{bm} + T_{mi} + T_{ir}. \quad (1)$$

Note that positive T_{sr} is defined as the observed part of the ionosphere lagging behind the IMF at the satellite.

In this paper, we take T_{mi} to be a single Alfvén wave travel time from the magnetopause to the ionosphere.

TABLE 1. SATELLITE LOCATIONS, OBSERVED IMF COMPONENTS (GSE CO-ORDINATES), AND PREDICTED SATELLITE-TO-RADAR LAGS (T_{sr}) FOR TIMES OF FLOW-BURST EVENTS NUMBERED IN FIG. 4

Event number	U.T. of peak Φ (h:min)	X_s (R_E)	Y_s (R_E)	B_x (nT)	B_y (nT)	T_{sr} (min)
1	09:06	−4.7	−34.2	−10.8	8.3	−3
2	09:16	−4.8	−34.1	−12.5	11.8	−1
3	09:23	−4.4	−33.7	−8.9	15.2	3
4	09:32	−4.4	−33.7	−8.4	15.9	4
5	09:53	−4.1	−34.1	−6.6	17.8	6
6	10:18	−3.9	−34.1	−1.9	15.2	8
7	10:35	−3.6	−34.1	−4.0	13.0	6
8	10:51	−3.4	−34.0	−8.3	16.0	4
9	11:08	−3.2	−34.0	−10.0	9.5	0

Freeman *et al.* (1990) compute this value for the L-shell of the centre of the CP-4 field of view at noon to be $T_{mi} = 2$ min (± 0.6 min) from the field-line resonance studies by Samson and Rostoker (1972).

In considering T_{bm}, let the speed of plasma flow in the undisturbed solar wind be V_{SW} and the average speed in crossing the subsolar magnetosheath be $\langle V_{sh} \rangle$. If X_b and X_m are the X coordinates of the subsolar bow shock and magnetopause, respectively, then

$$T_{bm} = (X_b - X_m)/\langle V_{sh} \rangle. \quad (2)$$

Following the results of Spreiter and Stahara (1980) we take

$$\langle V_{sh} \rangle = V_{sw}/8, \quad (3)$$

and from Fairfield (1971) we use the approximation for the subsolar stand-off distance of the bow shock:

$$X_b = 1.33 X_m. \quad (4)$$

To calculate the delay T_{sb}, we need to know the plane in which a discontinuity or gradient in B_z lies in interplanetary space. Following the results of Kelly *et al.* (1986), we here assume that such changes in B_z are aligned with the field vector in the ecliptic plane. Using the construction shown in Fig. 8, and assuming the X and Y coordinates of *IMP*-8 (X_s, Y_s) are such that $|Y_s/X_s| \gg 1$ (so that the change in B_z approximately impinges upon the bow-shock at $Y = 0$, $X = X_b$), and that the B_x- and B_y-components of the IMF are constant between the satellite and the sub-solar bow shock, we derive

$$T_{sb} \approx \{X_s - X_b - (Y_s \cdot B_x/B_y\}/[\{\cos\delta + (\sin\delta \cdot B_x/B_y)\} \cdot V_{sw}]. \quad (5)$$

For the period of interest here it is a good approxi-

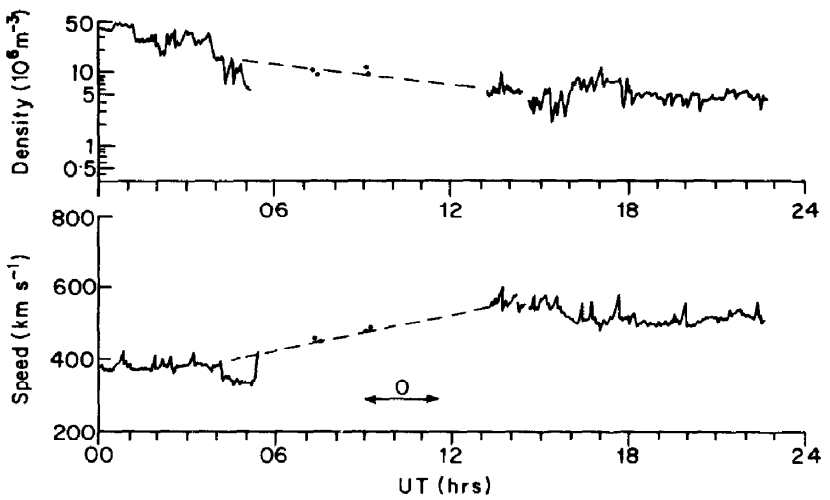

FIG. 9. SOLAR WIND SPEED AND DENSITY OBSERVED BY *IMP*-8 ON 12 JANUARY 1988.

mation to take the angle δ to be zero, and then the denominator in (5) reduces to V_{sw}. From equations (1)–(5) we then have:

$$T_{sr} = [X_s - 1.33X_m - (Y_s \cdot B_x/B_y) + 2.64X_m]/V_{sw} + T_{ir} + 120(s). \quad (6)$$

Hence to predict the lag T_{sr} we need the interpolated value of solar wind speed and a predicted location for the subsolar magnetopause. For an equilibrium position, the stand-off distance of the magnetopause is inversely proportional to RAM pressure:

$$X_m = G/[n_{sw}V_{sw}^2]^{1/6} \quad (7)$$

where n_{sw} is the solar wind density and G is a scaling factor.

In this paper we estimate the delay T_{ir} by making use of two features in the radar vector data which can be associated with changes in the IMF seen by *IMP*-8 (see Lockwood *et al.*, 1989b). The first is a northward turning of the IMF at 11:23 U.T., seen by EISCAT as a slowing of the flow commencing at 11:15 U.T. (note T_{sr} is negative because $B_x/B_y \approx -2$ before 11:22:30): the second is a southward swing of the IMF and change in sense of B_y, seen by *IMP*-8 at 11:25, but not observed as an increase in flows at EISCAT until 11:30 U.T. [between these two events the estimate of T_{sr} changed sense, mainly because of a change in the third term in the numerator of equation (5), B_x/B_y being ≈ 0.5 after 11:22:30]. Applying equations (6) and (7) to these two events gives two sets of equations from which we can derive both G and T_{ir}. The value obtained for G of $135R_E$ (Earth radii) is very similar to that derived by Farrugia *et al.* (1989) from *ISEE* observations of a static magnetopause, under similar solar wind flow conditions and is close to the mean value derived from the results of Holzer and Slavin (1978). This places the subsolar magnetopause at $11R_E$ at 09:00 U.T., consistent with the inferred proximity of *IMP*-8 to the bow shock. The delay T_{ir} is 3.0 min. The origin of this delay for a southward turning of the IMF (observed using EISCAT with the *AMPTE-UKS* satellite) has been discussed by Lockwood *et al.* (1986) and shown to be due to the expansion of a new, enhanced convection pattern from the ionospheric projection of the merging neutral line to the radar field-of-view. These authors showed that the region of ion frictional heating, caused by the enhanced convection, was indeed propagating over the radar at the required speed. In this paper, we assume that G and T_{ir} both remain constant during the 2.5-h period studied. The value for T_{ir} derived from the southward and northward turning should be valid at the end of this period. Study

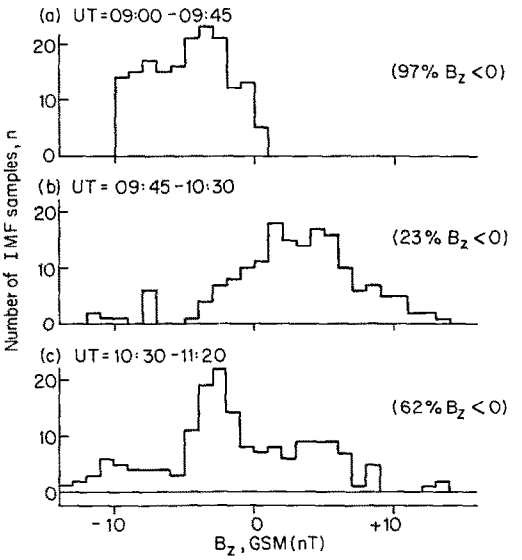

FIG. 10. HISTOGRAMS OF OCCURRENCE OF IMF B_z FOR THREE PERIODS ON 12 JANUARY 1988.
(a) 09:00–09:45 U.T., (b) 09:45–10:30 U.T. and (c) 10:30–11:20 U.T.

of the optical events tells us that the same value is reasonable even early in the period; for example, the all-sky images show that events 1 and 2 originate to the east of the TV cameras' field-of-view, i.e. somewhere further than 500 km to the east of the radar field-of-view. At the observed initial westward velocity of 3 km s^{-1}, the delay of T_{ir} of 3.0 min would place the point of origin at 540 km to the east of the radar field-of-view [see Fig. 2e and full sequence presented in part (f) of Fig. 2]. In practice, we would expect T_{ir} to decrease with U.T. as the radar rotates eastward and hence the value of 3.0 min could be an underestimate for the earlier events. This point will be raised again in Section 3.

From equations (6) and (7), we can now estimate the lag T_{sr} between an observation of the IMF at *IMP*-8 and each of the event times given in Table 1. There are a large number of approximations in this calculation and the answer is expected to be accurate only to within about 2.5 min, roughly the same error as in the timing of the event itself (see previous section). The lags are given in Table 1 and show considerable variation, mainly caused by changes in the ratio B_x/B_y, due to the large value of $|Y_s|$.

3. RESULTS

Figure 10 gives the distribution of the northward (B_z)-component of the IMF in GSM coordinates, for three subperiods of the interval discussed in this

paper. Part (a) shows that the IMF was almost continuously southward during 09:00–09:45, with only four of the 15-s samples in this period giving a slightly northward IMF (all of which were smaller than 1 nT and occurred at the very end of the period). Table 1 shows that there are four clear optical/radar transient events during this period, giving three estimates of the repetition period. The mean of these is 8.7 min, with a standard error in the mean of 0.9 min. In addition, there is the possible event *X*, which was revealed by the Hornsund magnetometer data but is also probably present in the radar and optical data. This event is 7.5 min after event 4, and its inclusion makes the mean 8.3 min with a standard error of 0.6.

During 09:45–10:30, the IMF was predominantly northward, with only 23% of samples giving a southward orientation of the total field vector [see part (b) of Fig. 10]. During this period only two events were observed, separated by 25 min.

The third subperiod [10:30–11:20 U.T., part (c) of Fig. 10] shows a more equal number of positive and negative B_z values, in fact 62% of IMF samples are southward. Within this period, three events are observed, separated by 16 and 17 min.

Combining periods (b) and (c), we find a mean recurrence period of 19.2 min with a standard error in that mean of 1.7 min. Hence, we find that the period 09:00–09:45, when the IMF was continuously southward, has a significantly shorter repetition period, than the subsequent periods, when the IMF varied between southward and northward.

In order to investigate these periods in more detail, Fig. 11 shows the IMF B_z- and B_y-components as a function of the U.T. at which they were observed by *IMP*-8. Also shown is the variation of Φ observed by EISCAT, but plotted as a function of the U.T. of observation minus the computed lag T_{sr}. The arrows show the peaks of the clear events, as listed in Table 1, and the event *X*. It is hard to identify a consistent trigger for the events in the IMF data. On the other hand, neither B_z nor B_y are constant. Sandholt *et al.* (1989b) note that events 1 and 2 differ considerably in their motion—event 1 having a much weaker initial westward moving phase. Allowing for the predicted lag T_{sr}, these two events are seen to follow periods of very similar B_z, but event 1 could have been reconnected during the brief period of small B_y (roughly 4 nT) around 09:07 U.T. This would explain its weaker westward motion compared with event 2 (for which the corresponding B_y is roughly 10 nT) and indeed with all subsequent events. Event 2 shows no clear trigger but event 3 could be associated with the rapid decrease in B_z after 09:17 U.T. If this association is real, event 3 could be said to be consistent with the Southwood *et al.* (1988)/Scholer (1988) concept of FTE generation by variations in reconnection rate, in this case induced by external fluctuations in IMF B_z. However, event 4 also has no clear trigger of any kind, occurring within a period of gradually increasing, but still negative B_z. The event *X* could be associated with a brief swing to more negative B_z around 09:32 U.T. Note that events 1–4 and *X* do not appear to be regularly spaced in Fig. 11 because of variations in T_{sr}. However, Figs 4 and 6 and Table 1 show that separation of the events in the ionosphere is comparatively constant. It seems highly unlikely that the variation in T_{sr} should act to cancel the variation in repetition period of irregular IMF triggers to give a nearly regular series of events in the ionosphere. We therefore think that these data imply a natural period of about 8 min which is a characteristic of the magnetospheric system.

Figure 12 shows the IMF B_z-component and the radar potential shifted by T_{sr}, as in Fig. 11, for the subsequent periods [(b) and (c) in Fig. 10]: B_y is not shown as it remained almost constant at about 15 nT after 09:20 U.T. Without the lags listed in Table 1, events 5, 6 and 7 were all observed when the field observed simultaneously by *IMP*-8 is positive. However, Fig. 7 shows that with the computed lags T_{sr} introduced, each event coincides, or follows shortly after, a swing (often short-lived) to southward IMF. Remembering the errors in the event timings and in the lag estimates, we cannot definitively associate each event with a period of southward IMF; however, we can say that each burst of southward IMF could have triggered an "isolated" transient flow burst and auroral event. It is noticeable that it is the earlier events, 5 and 6, which do not exactly coincide with the southward swings. This could, as discussed in the previous section, be due to the fact that 3 min is an underestimate of T_{ir} for these events, or because for these two events $|B_y/B_x|$ is exceptionally large (see Table 1), exposing a deficiency in our assumptions in the calculation of T_{sb}.

Supporting evidence for the above conclusions is given in Fig. 13, which plots the potential, Φ, across the North–South extent of the radar field-of-view (solid circles) as a function of average B_z for a 2-min period around the associated minimum in B_z. A clear relationship can be seen, with larger potentials produced for events during more southward IMF. The only event which does not follow this trend well is event 1. As discussed earlier, this event does not move strongly westward initially, as do the other eight events, but rather moves directly poleward into the polar cap. Also shown in Fig. 13 are the peak potentials associated with northward motions of the events

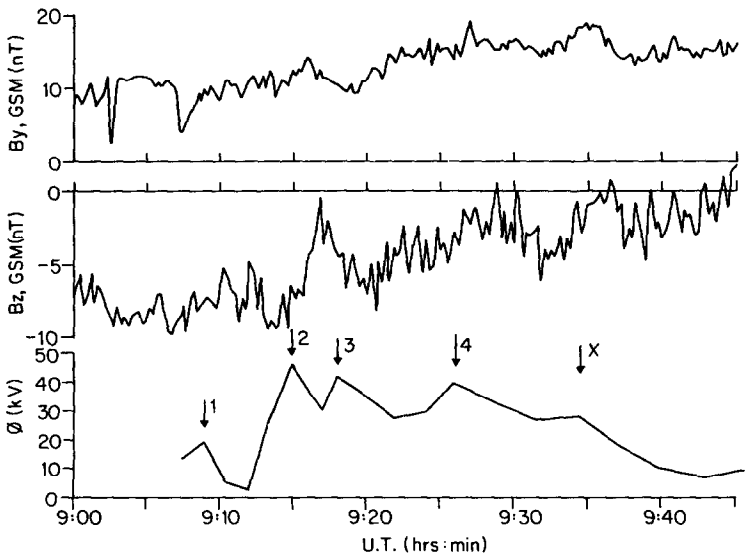

FIG. 11. IMF B_z- AND B_y-COMPONENTS AND RADAR POTENTIAL, Φ, AS A FUNCTION OF U.T. ON 12 JANUARY 1988.
The radar values have been advanced by the estimated delay for IMF effect to reach the radar field-of-view, T_{sr} (see Table 1) and events have been numbered as in Fig. 4.

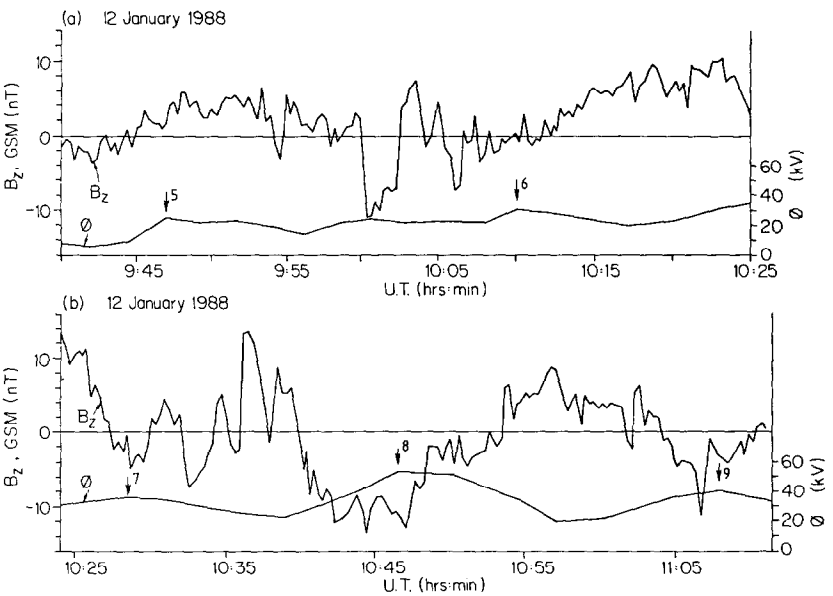

FIG. 12. IMF B_z AND RADAR POTENTIAL, Φ, AS A FUNCTION OF U.T. ON 12 JANUARY 1988.
As for Fig. 11, the radar values have been advanced by the estimated delay for IMF effect to reach the radar field-of-view, T_{sr} (see Table 1) and events have been numbered as in Fig. 4.

(i.e. measured across the East–West dimension of the radar field-of-view), Φ_e (open circles). These also show a slight trend to increase with more negative IMF B_z. However, it is known that these Φ_e values are underestimates because the all-sky TV images define the auroral luminosity as extending further in the East–West direction than the radar field-of-view. These TV observations show that the potential associated with the poleward motion of the visible arc of event 1 is 35 kV. The total potential associated with

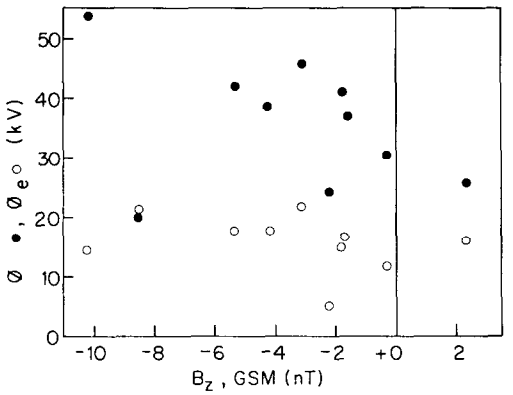

FIG. 13. PEAK RADAR POTENTIALS (LAGGED BY T_{sr}) AS A FUNCTION OF MEAN IMF B_z.
The potential across the North–South dimension of the radar field-of-view (corresponding to westward flow), Φ, is shown by solid circles, that across the East–West dimension (corresponding to northward flow), Φ_e, by open circles.

this event must exceed this value because the event could be larger than the arc detected by the TV camera.

4. DISCUSSION AND CONCLUSIONS

We have studied the only available simultaneous radar/optical data of transient bursts of ionospheric ion flow in the cleft region, accompanied by the "dayside auroral breakup" transient auroral activity. From these limited data we find that the bursts occur quasi-periodically when the IMF is strongly and continuously southward. However, during periods of intermittant southward IMF, the external field can trigger "isolated" events. In this section we will discuss these two types of IMF conditions separately in Sections 4.1 and 4.2, before looking at the implications of the optical event lifetimes for the motion of newly opened flux tubes in Section 4.3. When reading all three of these subsections, it must be remembered that they are based on only a very short period of observation. It is vital that further observations be made to give the results the same statistical weight as the extensive surveys of magnetopause data.

4.1. *Observations during continuous southward IMF*

The mean period of the events when the IMF was continuously southward (09:00–09:43 U.T.) is 8.3 ± 0.6 min (including event *X*). This repetition period is very similar to the mean period between FTEs at the magnetopause under the same IMF conditions [Rijnbeek *et al.* (1984) found a value of 7 min for FTEs]. This is also consistent with earlier studies of the transient dayside aurorae, without the radar data (see Fig. 1).

We consider the evidence that the transient arcs are indeed the clearest ionospheric signature of FTEs to be overwhelming. Briefly summarizing that evidence (other than the repetition period and occurrence seemingly only during southward IMF), we note that events (as yet documented in detail for the Northern Hemisphere only) move westward when IMF B_y is positive and eastward when it is negative (Sandholt *et al.*, 1989a; Sandholt, 1988) and are accompanied by spikes in magnetometer records, the sense of which depend also on IMF B_y (Oguti *et al.*, 1988). The directions of these motions are as predicted for newly-opened flux tubes under magnetic tension due to the B_y-component of the IMF (Jørgensen *et al.*, 1972; Cowley, 1981). The events are seen to move initially rapidly West/East before turning poleward and moving at more typical convection speeds (Lockwood *et al.*, 1989a; Sandholt *et al.*, 1989b), consistent with the motion of newly-reconnected flux tubes predicted by Lockwood and Freeman (1989) and Saunders (1989). This two-phase motion arises from the actions of magnetic tension and anti-solar solar wind flow: the tension induces ionospheric flow an Alfvén wave travel time after reconnection at the magnetopause, whereas the anti-solar flow does not begin to excite ionospheric flow until a few minutes later when the flux tube has straightened. The event lifetimes (2–15 min) are consistent with the periods during which momentum is transferred to the ionosphere following the formation of an open flux tube at the dayside magnetosphere (Lockwood and Cowley, 1988; Lockwood and Freeman, 1989; Lockwood *et al.*, 1989b). The ionospheric flows around these events and the inferred and measured field-aligned currents have been shown to be consistent with those predicted for FTEs by Southwood (1985, 1987) and Southwood *et al.* (1988) and Cowley (1984, 1986) (Lockwood *et al.*, 1989a; Sandholt *et al.*, 1989b,c; Sandholt and Egeland, 1988).

In addition, the events show strong green-line emissions, hence we know that the precipitating particles are not merely solar wind particles that have entered the magnetosphere and are precipitated into the ionosphere without further acceleration. It should be noted that these transient green-line arcs are observed throughout the dayside, with no midday gap, as observed for more stable arcs—hence they occur in both the "cusp" and "cleft" regions (Heikkila, 1985). We considered whether the origin of these heated particles could be the streaming hot electrons observed on the flanks of FTEs on the magnetopause (Scudder *et al.*, 1984). However, such electrons only have energies of a few hundreds of electronvolts,

whereas kiloelectronvolt particles are required to explain the photometer observations (Sandholt *et al.*, 1989a). Hence it is thought that a transient and localized potential difference may be formed between the ionosphere and the magnetopause during these events associated with the upward field-aligned current (Sandholt *et al.*, 1989b). Recently, Lockwood and Smith (1989) have interpreted a cusp ion injection event, observed at 900 km by *DE*-2, as an FTE and found that the observed perturbation electric and magnetic fields were also consistent with a Southwood (1987) FTE model and that precipitating electrons of energy ~ 100 eV were indeed present on the boundaries of the putative newly-opened flux tube, as for the magnetopause observations. However, in this case *DE*-2 did not pass through or near the region of upward field-aligned current and hence did not see the particles responsible for the green-line transient arc.

4.2. *Observations during intermittent southward IMF*

After 09:48 U.T., the IMF observed by *IMP*-8 was predominantly northward, with only brief periods of southward orientation. If the predicted lag, T_{sr}, between the IMF impinging upon the satellite and its effects reaching the ionosphere within the radar field-of-view are not taken into account, many of the transient flow/auroral events seem to occur during northward IMF. However, with the best possible estimates of this lag included, we can say that, to within the errors of the observations and the predicted lags, each event could have been triggered by a southward swing of the IMF. Indeed, the potential of the event (in its initial, westward-moving phase) is found to correlate well with the B_z during the swing it is thought to be associated with. Under these conditions, the mean period between the events is significantly longer and is seemingly controlled by the variability of the IMF B_z-component. Notice this is a very different situation from that described in Section 4.1, where the periodicity seems to be due to some internal magnetospheric "clock", and not to variations in the IMF.

4.3. *Motion of newly opened flux tubes*

Figure 2 shows that the optical event onsets at the meridian scanned by the photometers is earlier for the 630 nm emissions than for 557.7 nm and that the radar potential increases before both of these times. This suggests that the softer particles responsible for the 630 nm luminosity are precipitated over a larger region than those causing the 557.7 green-line emissions. Lockwood *et al.* (1989a) postulate that the green-line emissions mark the region of upward field-aligned current of the oppositely-directed pair required to transfer momentum to the ionosphere, a conclusion supported by the more detailed analysis presented by Sandholt *et al.* (1989b). The red-line emissions could be seen over a larger region if they were present throughout the newly opened flux tube, as expected for entry of solar wind particles by reconnection (see Lockwood and Smith, 1989). The flows are expected to respond first, as closed field-lines or "old" open field-lines are effectively pushed ahead of the event in the Southwood model of FTE signatures (see Lockwood *et al.*, 1988 and Fig. 7).

Lockwood *et al.* (1989a) and Sandholt *et al.* (1989b) have shown that the motion of the optical events (and the simultaneously-observed ion flows) are consistent with the predictions of Lockwood and Freeman (1989) and Saunders (1989). This is because the events initially move westward under magnetic tension (IMF B_y was positive), before swinging round to more poleward flow as anti-solar motion begins to become effective and East–West magnetic tension decreases. Saunders (1989) has also shown how this motion naturally explains the cusp field-aligned currents and hence we believe the filamentary currents of one of the larger events could be thought of as a travelling intensification of the region one-cusp current system.

Figure 3 considers how this pattern of motion effects the lifetime, τ, of the optical events, as seen by a photometer scanning a single meridian (dashed line). From the all-sky TV images, we know that an event onset in the photometer data is caused by an auroral structure moving westward, crossing the meridian at time $t = 0$. However, for these observations at least, the end of each event is not because it moves westward past the meridian, but rather because it fades as it moves northward. By time $t = \tau$, the events are moving purely northward and the westward velocity has fallen to zero. The all-sky TV camera also tells us that the deceleration of the westward flow is roughly uniform for $t > 0$. For example, Table 2 gives the westward acceleration of the main patch of green-line luminosity, a, seen by the all-sky TV camera during event 2 [see Fig. 2(f) and Sandholt *et al.*, 1989b]. The mean value after 09:21:30 (when the high-luminosity patch reached the photometers' meridian) is $\langle a \rangle = -9.8$ m s^{-2}, with a standard error in that mean of only 0.12 m s^{-2}.

Hence we can apply the equation for constant acceleration to the open field-line of the event, marked by the red-line emissions, and from the definition of τ we have:

$$0 = V_{wo} + a\tau \tag{8}$$

where V_{wo} is the westward flow speed at $t = 0$ and a is the acceleration. In Fig. 5, τ was plotted as a func-

TABLE 2. ACCELERATION OF EVENT 2, AS OBSERVED BY THE ALL-SKY TV CAMERA AT NY ÅLESUND

U.T. (h : min : s)	Time, t (s)	Distance from position at time $t = \tau$ (s) (km)	$\tau - t$ (s)	Acceleration, $a = -2s/(\tau - t)^2$ (m s^{-2})
09:20:17	−74	340	203	−16.5
09:20:55	−36	182	165	−13.4
09:21:31	0	87	129	−10.4
09:22:00	29	48	100	−9.6
09:22:37	66	20	63	−10.1
09:22:58	87	8	42	−9.1
09:23:40	$129 = \tau$	0	0	—

tion of peak Φ, the radar potential near $t = 0$ associated with the initial westward motion. We can relate this Φ value with V_{wo} by

$$\Phi = V_{wo}BL \tag{9}$$

where L is the length along the meridian scanned by the radar where the flows are enhanced [Sandholt *et al.* (1989b) note that the flows are enhanced in a "channel" co-located with the persistent cusp/cleft aurora] and B is the magnetic induction in the ionosphere. Hence we have

$$\Phi = -aBL\tau. \tag{10}$$

This equation predicts that the data points in Fig. 5 should lie on a straight line if a is the same for every event. This agrees well with the data. Therefore this strengthens the association of the radar and optical data and supports the interpretation of the events given by Lockwood *et al.* (1989a) and Sandholt *et al.* (1989b).

From the observed slope of Fig. 5, and using a typical value for L of 150 km (corresponding to three range gates, see Fig. 2), we deduce that $a = -7.5$ m s^{-2}. This is the deceleration caused by the decrease of the driving B_y tension force, and is in general agreement with the mean value deduced above for $t > 0$ during event 2. That all these events have the same deceleration is because B_y (and hence the tension forces) and the background ionospheric conductivity (and hence the frictional drag) are roughly constant throughout the period.

Acknowledgements—The authors are grateful to R. Lepping and A. Lazarus, for their kind provision of *IMP*-8 magnetometer and particle flow data, respectively, and to the director and staff of EISCAT for their assistance: EISCAT is supported by the research councils of France (CNRS), West Germany (MPG), Norway (NAVF), Sweden (NFR), Finland (SA) and the U.K. (SERC). Financial support for the photometer and TV camera data is provided by Kyoikusha, LTD, NAVF and the Norwegian Polar Research Institute. We thank K. S. C. Freeman for processing the EISCAT data and B. Lybekk and B. Jacobson for processing the photometer observations.

REFERENCES

Berchem, J. and Russell, C. T. (1984) Flux transfer events at the magnetopause: spatial distribution and controlling factors. *J. geophys. Res.* **89**, 6689.

Cowley, S. W. H. (1981) Magnetospheric asymmetries associated with the Y-component of the IMF. *Planet. Space Sci.* **29**, 79.

Cowley, S. W. H. (1982) The causes of convection in the Earth's magnetosphere: a review of developments during IMS. *Rev. Geophys. Space Phys.* **20**, 531.

Cowley, S. W. H. (1984) Evidence for the occurrence and importance of reconnection between the Earth's magnetic field and the interplanetary magnetic field, in *Magnetic Reconnection in Space and Laboratory Plasmas* (Edited by Hones, E. W., Jr.), p. 375. Geophysical monograph 30, American Geophysical Union, Washington DC.

Cowley, S. W. H. (1986) The impact of recent observations on theoretical understanding of solar wind–magnetosphere interactions. *J. Geomagn. Geoelect.* **38**, 1223.

Eyken, A. P. van, Rishbeth, H., Willis, D. M. and Cowley, S. W. H. (1984) Initial EISCAT observations of plasma convection at invariant latitudes 70°–77°. *J. atmos. terr. Phys.* **46**, 635.

Etemadi, A., Cowley, S. W. H. and Lockwood, M. (1989) The effect of rapid change in ionospheric flow on velocity vectors deduced from radar beamswinging experiments. *J. atmos. terr. Phys.* **51**, 125.

Fairfield, D. H. (1971) Average and unusual locations of the Earth's magnetopause and bow shock. *J. geophys. Res.* **76**, 6700.

Farrugia, C. J., Freeman, M. P., Cowley, S. W. H., Southwood, D. J., Lockwood, M. and Etemadi, A. (1989) Pressure-driven magnetopause motions and attendant response on the ground. *Planet. Space Sci.* **37**, 589.

Farrugia, C. J., Rijnbeek, R. P., Saunders, M. A., Southwood, D. J., Rodgers, D. J., Smith, M. F., Chaloner, C. P., Hall, D. S., Christiansen, P. J. and Wolliscroft, L. J. C. (1988) A multi-instrument study of flux transfer event structure. *J. geophys. Res.* **93**, 14,465.

Freeman, M. P., Farrugia, C. J., Cowley, S. W. H. and

Etemadi, A. (1990) The response of dayside ionospheric convection to the *Y*-component of the magnetosheath magnetic field: a case study. *Planet. Space Sci.* (in press).

Goertz, C. K., Neilsen, E., Korth, A., Glassmeier, K.-H., Haldoupis, C., Hoeg, P. and Hayward, D. (1985) Observations of a possible signature of flux transfer events. *J. geophys. Res.* **90**, 4069.

Haerendel, G., Paschmann, G., Sckopke, N., Rosenbauer, H. and Hedgecock, P. C. (1978) The frontside boundary layer of the magnetosphere and the problem of reconnection. *J. geophys. Res.* **83**, 3195.

Heelis, R. A. (1984) The effects of the interplanetary magnetic field orientation on dayside high-latitude convection. *J. geophys. Res.* **89**, 2873.

Heikkila, W. (1985) Definition of the cusp, in *The Polar Cusp* (Edited by Holtet, J. A. and Egeland, A.), p. 387. D. Reidel, Dordrecht.

Holzer, R. E. and Slavin, J. A. (1978) Magnetic flux transfer associated with expansions and contractions of the dayside magnetopause. *J. geophys. Res.* **83**, 3831.

Jørgensen, T. S., Friis-Christensen, E. and Wilhjelm, J. (1972) Interplanetary magnetic field direction and high-latitude ionospheric currents. *J. geophys. Res.* **77**, 1976.

Kelly, T. J., Crooker, N. U., Siscoe, G. L., Russell, C. T. and Smith, E. J. (1986) On the use of sunward libration-point-orbiting spacecraft as an interplanetary magnetic field monitor for magnetospheric studies. *J. geophys. Res.* **91**, 5629.

Kokubun, S., Yamamoto, T., Hayashi, K., Oguti, T. and Egeland, A. (1988) Impulsive Pi bursts associated with poleward moving auroras near the polar cusp. *J. Geomagn. Geoelect.* **40**, 537.

Lanzerotti, L., Hunsucker, R. D., Rice, D., Lee, L. C., Wolfe, A., Maclennan, C. G. and Medford, L. V. (1987) Ionosphere and ground-based response to field-aligned currents near the magnetospheric cusp region. *J. geophys. Res.* **92**, 7739.

Lee, L. C. and Fu, Z. F. (1985) A theory of magnetic flux transfer at the Earth's magnetopause. *Geophys. Res. Lett.* **12**, 105.

Lee, L. C., Shi, Y. and Lanzerotti, L. (1988) A mechanism for the generation of cusp region hydromagnetic waves. *J. geophys. Res.* **93**, 7578.

Lockwood, M. and Cowley, S. W. H. (1988) Observations at the magnetopause and in the auroral ionosphere of momentum transfer from the solar wind. *Adv. Space Res.* **8**, 281.

Lockwood, M., van Eyken, A. P., Bromage, B. J. I., Willis, D. M. and Cowley, S. W. H. (1986) Eastward propagation of a plasma convection enhancement following a southward turning of the interplanetary magnetic field. *Geophys. Res. Lett.* **13**, 72.

Lockwood, M. and Freeman, M. P. (1989) Recent ionospheric observations relating to solar wind–magnetosphere coupling. *Phil. Trans. R. Soc., London A.* **328**, 93.

Lockwood, M. and Smith, M. F. (1989) Low-altitude signatures of the cusp and flux transfer events. *Geophys. Res. Lett.* **16**, 879.

Lockwood, M., Smith, M. F., Farrugia, C. J. and Siscoe, G. L. (1988) Ionospheric ion upwelling in the wake of flux transfer events at the dayside magnetopause. *J. geophys. Res.* **93**, 5641.

Lockwood, M., Sandholt, P. E. and Cowley, S. W. H. (1989a) Dayside auroral activity and magnetic flux transfer from the solar wind. *Geophys. Res. Lett.* **16**, 33.

Lockwood, M., Cowley, S. W. H. and Freeman, M. P. (1989b) The excitation of ionospheric convection. *J. geophys. Res.* (in press).

McHenry, M. A. and Clauer, C. R. (1987) Modeled ground magnetic signatures of flux transfer events. *J. geophys. Res.* **92**, 11231.

Oguti, T., Yamamoto, T., Hayashi, K., Kokubun, S., Egeland, A. and Holtet, J. A. (1988) Dayside auroral activities and related magnetic impulses in the polar cusp region. *J. Geomagn. Geoelect.* **40**, 387.

Rijnbeek, R. P., Cowley, S. W. H., Southwood, D. J. and Russell, C. T. (1984) A survey of dayside flux transfer events observed by the *ISEE*-1 and -2 magnetometers. *J. geophys. Res.* **89**, 786.

Russell, C. T. and Elphic, R. C. (1978) Initial *ISEE* magnetometer results: magnetopause observations. *Space Sci. Rev.* **22**, 681.

Russell, C. T. and Elphic, R. C. (1979) *ISEE* observations of flux transfer events at the dayside magnetopause. *Geophys. Res. Lett.* **6**, 33.

Samson, J. C. and Rostoker, G. (1972) Latitude-dependent characteristics of high-latitude Pc4 and Pc5 micropulsations. *J. geophys. Res.* **77**, 6133.

Sandholt, P. E. (1988) IMF control of the polar cusp and cleft auroras. *Adv. Space Res.* **8**, 21 34.

Sandholt, P. E. and Egeland, A. (1988) Auroral and magnetic variations in the polar cusp and cleft-signatures of magnetopause boundary layer dynamics. *Astrophys. Space Sci.* **144**, 171.

Sandholt, P. E., Egeland, A., Holtet, J. A., Lybekk, B., Svenes, K. and Asheim, S. (1985) Large- and small-scale dynamics of the polar cusp. *J. geophys. Res.* **90**, 4407.

Sandholt, P. E., Lybekk, B., Egeland, A., Nakamura, R. and Oguti, T. (1989a) Midday auroral breakup. *J. Geomagn. Geoelect.* (in press).

Sandholt, P. E., Lockwood, M., Oguti, T., Cowley, S. W. H., Freeman, K. S. C., Lybekk, B., Egeland, A. and Willis, D. M. (1989b) Midday auroral breakup events and related energy and momentum transfer from the magnetosheath. *J. geophys. Res.* (in press).

Sandholt, P. E., Lybekk, B., Egeland, A., Jacobson, B., Bythrow, P. F. and Hardy, D. A. (1989c) Electrodynamics of the polar cusp ionosphere—a case study. *J. geophys. Res.* **94**, 6713.

Saunders, M. A., Russell, C. T. and Sckopke, N. (1984) A dual-satellite study of spatial properties of FTEs, in *Magnetic Reconnection in Space and Laboratory Plasmas* (Edited by Hones, E. W., Jr.), p. 145. Geophysical monograph 30, American Geophysical Union, Washington DC.

Saunders, M. A. (1989) The origin of cusp Birkeland currents. *Geophys. Res. Lett.* **16**, 151.

Scholer, M. (1988) Magnetic flux transfer at the magnetopause based on single X-line bursty reconnection. *Geophys. Res. Lett.* **15**, 291.

Scudder, J. D., Ogilvie, K. W. and Russell, C. T. (1984) The relationship of flux transfer events to magnetic reconnection, in *Magnetic Reconnection in Space and Laboratory Plasmas* (Edited by Hones, E. W., Jr.), p. 153. Geophysical monograph 30, American Geophysical Union, Washington DC.

Sibeck, D. G., Baumjohann, W. and Lopez, R. E. (1989) Solar wind dynamic pressure variations and transient magnetospheric signatures. *Geophys. Res. Lett.* **16**, 13.

Southwood, D. J. (1985) Theoretical aspects of ionosphere–magnetosphere–solar wind coupling. *Adv. Space Res.* **5**, 7.

Southwood, D. J. (1987) The ionospheric signature of Flux Transfer Events. *J. geophys. Res.* **92**, 3207.

Southwood, D. J., Saunders, M. A., Dunlop, M. W., Mier-Jedrzejowicz, W. A. C. and Rijnbeek, R. P. (1986) A survey of Flux Transfer Events recorded by *UKS* spacecraft magnetometer. *Planet. Space Sci.* **34**, 1349.

Southwood, D. J., Farrugia, C. J. and Saunders, M. A. (1988) What are flux transfer events? *Planet. Space Sci.* **36**, 503.

Spreiter, J. R. and Stahara, S. S. (1980) A new predictive model for determining solar wind–terrestrial planetary interactions. *J. geophys. Res.* **85**, 6769.

Todd, H., Bromage, B. J. I., Cowley, S. W. H., Lockwood, M., van Eyken, A. P. and Willis, D. M. (1986) EISCAT observations of bursts of rapid flow in the high latitude dayside ionosphere. *Geophys. Res. Lett.* **13**, 909.

Todd, H., Cowley, S. W. H., Etemadi, A., Bromage, B. J. I., Lockwood, M., Willis, D. M. and Luhr, H. (1988) Flow in the high-latitude ionosphere: measurements at 15-second resolution using the EISCAT "Polar" experiment. *J. atmos. terr. Phys.* **50**, 423.

Willis, D. M., Lockwood, M., Cowley, S. W. H., Rishbeth, H., van Eyken, A. P., Bromage, B. J. I., Smith, P. R. and Crothers, S. R. (1986) A survey of simultaneous observations of the high latitude ionosphere and interplanetary magnetic field with EISCAT and *AMPTE-UKS*. *J. atmos. terr. Phys.* **48**, 987.